The Journal of Chemical Physics

RESEARCH ARTICLE | MARCH 20 2024

Impact of large A-site cations on electron–vibrational interactions in 2D halide perovskites: *Ab initio* quantum dynamics

Special Collection: Festschrift in honor of Louis E. Brus

Dandan Dai; Sraddha Agrawal ; Oleg V. Prezhdo ; Run Long

J. Chem. Phys. 160, 114704 (2024)
https://doi.org/10.1063/5.0202251
CHORUS

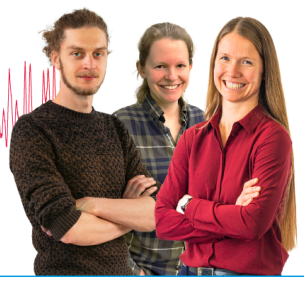

The Journal of Chemical Physics ARTICLE pubs.aip.org/aip/jcp

Impact of large A-site cations on electron–vibrational interactions in 2D halide perovskites: *Ab initio* quantum dynamics

Cite as: J. Chem. Phys. 160, 114704 (2024); doi: 10.1063/5.0202251
Submitted: 2 February 2024 • Accepted: 3 March 2024 •
Published Online: 20 March 2024

Dandan Dai,[1] Sraddha Agrawal,[2] Oleg V. Prezhdo,[2,a)] and Run Long[1,a)]

AFFILIATIONS

[1] College of Chemistry, Key Laboratory of Theoretical and Computational Photochemistry of Ministry of Education, Beijing Normal University, Beijing 100875, People's Republic of China
[2] Department of Chemistry, University of Southern California, Los Angeles, California 90007, USA

Note: This paper is part of the JCP Festschrift in honor of Louis E. Brus.
[a)] **Authors to whom correspondence should be addressed:** prezhdo@usc.edu and runlong@bnu.edu.cn

ABSTRACT

Using *ab initio* nonadiabatic molecular dynamics, we study the effect of large A-site cations on nonradiative electron–hole recombination in two-dimensional Ruddlesden–Popper perovskites $HA_2APb_2I_7$, HA = n-hexylammonium, A = methylammonium (MA), or guanidinium (GA). The steric hindrance created by large GA cations distorts and stiffens the inorganic Pb–I lattice, reduces thermal structural fluctuations, and maintains the delocalization of electrons and holes at ambient and elevated temperatures. The delocalized charges interact more strongly in the GA system than in the MA system, and the charge recombination is accelerated. In contrast, replacement of only some MA cations with GA enhances disorder and increases charge lifetime, as seen in three-dimensional perovskites. This study highlights the key influence of structural fluctuations and disorder on the properties of charge carriers in metal halide perovskites, providing guidance for tuning materials' optoelectronic performance.

I. INTRODUCTION

Solar cell and optoelectronic communities have witnessed a rapid development of hybrid organic–inorganic halide perovskites (HOIPs), which enable efficient and affordable solar cells.[1,2] In the past twelve years, the power conversion efficiency of perovskite solar cells has increased from 3.8%[3] to 25.5%.[4] The development makes it the most promising photovoltaic technology, mainly due to the unique properties of halide perovskites,[5] such as high absorption coefficient,[6–8] long carrier diffusion length,[9–12] low trap state density,[13,14] large carrier mobility,[15,16] and low exciton binding energy.[17] The crystal structure of three-dimensional (3D) halide perovskites with the general formula ABX_3 [A = Cs, methylammonium (MA), formamidinium (FA); B = Pb, Sn, Ge; X = Cl, Br, I][18] includes corner-sharing $[PbX_6]^{4-}$ octahedra and A cations occupying 12-fold coordinating cavities formed by eight adjacent octahedra. 3D perovskites form diverse structures,[16,19,20] within the limits quantified by the Goldschmidt tolerance factor (t).[21,22] For lead iodide perovskite $APbI_3$, $t = (r_A + r_I)/\left[\sqrt{2}/(r_{Pb} + r_I)\right]$, in which r_A, r_{Pb}, and r_I are the effective radii of A, Pb, and I ions. Only when this value is between 0.8 and 1, the perovskite phase can be observed. When the t value is greater than 1 or less than 0.8, non-perovskite phases are formed.[23] Therefore, large cations such as guanidinium (GA), ethylammonium (EA), or dimethylammonium (DMA), leading to tolerance factors greater than 1, cannot be used as A-site cations in 3D perovskites. Increasing the variety and improving the structural stability of perovskites, two-dimensional Ruddlesden–Popper (2DRP) perovskites are obtained by incorporating large organic molecules as spacer cations to separate layers of the inorganic framework of the 3D perovskites.[24,25] 2DRP perovskites can be described as $(LA)_2(A)_{n-1}Pb_nI_{3n+1}$, where LA is a spacer cation and A represents an A-site cation. Because the flexible spacer cations can withstand the strain caused by A cations,[26,27] 2DRP perovskites allow for the formation of large-size A cation perovskites.

Basic insights into structure–property relationships are key to understanding the properties of charge carriers in HOIPs. Regulating the structure and functional diversity of perovskites can have a

strong impact on carrier mobility, relaxation, and lifetimes. There have been theories on how organic cations affect the charge separation and recombination and ferroelectricity in perovskites.[28–30] For example, He *et al.* demonstrated that doping $MAPbI_3$ with a small amount of GA cations can prolong the charge carrier lifetime and improve the photoelectric performance,[31] rationalizing experiments.[32,33] However, fully GA-based 3D perovskites cannot be generated due to the tolerance factor limitation, restricting performance research. The relaxation of the range of the Goldschmidt tolerance factor in 2DRP perovskites allows a broader tuning of A-site cation size in search of improved performance. Fu *et al.* obtained the $HA_2GAPb_2I_7$ (HA = n-hexylammonium) single crystal structure for the first time,[27] confirming that the large-size GA cations can exist in two-dimensional perovskite cavities. Using the time-resolved photoluminescence (PL) spectra, the authors established that the average PL lifetimes of $HA_2MAPb_2I_7$ and $HA_2GAPb_2I_7$ were 114 ± 6 and 54 ± 6 ps, respectively, indicating that the incorporation of large A cations had an impact on the excited state lifetime. Experiments showed that the incorporation of GA caused the volume of the perovskite cavities to increase and the distance between the inorganic layers to reduce, which induced a blue shift of the bandgap and shortened the PL lifetime. Soon after, Hautzinger and colleagues explored the evolution of the bandgap with cations of different sizes in the 2DRP perovskite $HA_2APb_2I_7$ (A = MA, FA, GA, and EA),[34] demonstrating a structure–performance relationship similar to that in the previous experiment. At the same time, Li *et al.* proposed that the introduction of large A cations in $(BA)_2(A)Pb_2I_7$(A = MA, FA, DMA, and GA) produced a negative pressure in the perovskite cavities,[35] shortening the PL lifetime. Similar findings were reported in the same year by Fu *et al.*, who studied the effect of incorporating large A cations into $BA_2Apb_3I_{10}$ (A = MA and EA).[36] The above experiments showed that the introduction of large A cations into 2DRP perovskites has an adverse effect on its photovoltaic performance. This is in contrast to the earlier findings for 3D perovskites, in which incorporation of small amounts of large A-site cations leads to improved performance.[31–33] A theoretical rationalization of the above experimental observations can provide important insights into the fundamental properties and practical design of HOIPs. This goal can be achieved by *ab initio* quantum dynamics simulations, which allows one to reveal at the atomistic level the relationship of the geometric and electronic structure of a material and charge carrier dynamics.

Motivated by the recent experiments,[27,34–36] we combine time-dependent density functional theory (TDDFT)[37–39] and nonadiabatic molecular dynamics (NAMD)[40–45] to study the nonradiative electron–hole recombination in the $HA_2MAPb_2I_7$ and $HA_2GAPb_2I_7$ perovskites at the *ab initio* atomistic level of description and in the time domain. Our simulations show that the large GA cations create a steric hindrance and deform the perovskite cavities. The Pb–I bond length and the Pb–I–Pb bond angle increase, creating a deformation of the octahedral structure of the inorganic Pb–I lattice. The steric hindrance generated by the large GA cations reduces thermal structural fluctuations at ambient and elevated temperatures, maintaining the delocalization of HOMO and LUMO wavefunctions. Compared to the MA system, the electron and hole overlap more, and the NA coupling is increased in the GA perovskite. As a result, the charge carrier recombination is accelerated. The shorter carrier lifetime can have an adverse effect on the 2DRP perovskite performance. This study highlights the key role of structural fluctuations and disorder in defining the properties of charge carriers and performance of metal halide perovskites and provides guidelines for perovskite synthesis and performance tuning.

II. SIMULATION DETAILS

In order to study the effect of the incorporation of large A cations on the nonradiative electron–hole recombination in 2DRP perovskite systems, we performed hybrid quantum–classical NAMD[40–45] simulations, using the decoherence-corrected fewest-switches surface hopping (FSSH) technique[46–48] implemented within real-time TDDFT in the Kohn–Sham representation.[38,39] The lighter and faster electrons are described quantum mechanically, and the heavier and slower atoms are described semi-classically. The decoherence time is estimated in the NAMD simulation as the pure-dephasing time of the optical response theory.[49,50] Decoherence effects should be included into the current NAMD simulation because the decoherence time is significantly shorter than the electron–hole recombination time, and loss of quantum coherence has a strong effect on quantum transitions.[51] The approach has been used to study the photoexcitation dynamics in a broad range of systems, including 3D perovskites[52] with passivated surfaces[53] and grain boundaries,[54,55] 2D Dion–Jacobson perovskites,[56] transition metal dichalcogenides,[57–59] all-inorganic perovskite quantum dots,[60–62] black phosphorus,[63] graphitic carbon nitride,[64] etc.[65–69]

The geometry optimization, adiabatic molecular dynamics (MD), and nonadiabatic (NA) coupling calculations were performed using the Vienna *Ab initio* Simulation Package (VASP).[70] The Perdew–Burke–Ernzerhof (PBE) functional[71] was used to describe the electronic exchange and correlation interactions. The interactions between ionic cores and valence electrons were described by the projector-augmented wave (PAW) approach.[72] The structures were optimized by using the Γ-centered 3 × 3 × 1 Monkhorst–Pack k-point mesh[73] and a plane wave energy cutoff of 400 eV to achieve ion forces less than 10^{-3} eV $Å^{-1}$. The Grimme DFT-D3 method was used to describe the van der Waals interaction.[74] A much denser 6 × 6 × 2 k-point mesh was employed for electronic structure calculations. After geometry optimization at 0 K, both the systems were heated to 300 K by repeated velocity rescaling for 1 ps. Then, 6 ps adiabatic MD trajectories were generated for the two systems in the microcanonical ensemble with a 1 fs atomic time step. The NA couplings were computed[75,76] using the last 3 ps of the 6 ps trajectories and at the Γ point, since the direct bandgap of the systems was at the Γ point. Iterating the 3 ps of NA Hamiltonian four times, we performed 9 ps NAMD simulations using the 3000 geometries as initial conditions. Hundred realizations of the decoherence corrected FSSH algorithm[47,48] were sampled for each initial geometry.

III. RESULTS AND DISCUSSION

Figure 1 shows the optimized structures and representative structures at 300 K of the $HA_2MAPb_2I_7$ and $HA_2GAPb_2I_7$ systems. The crystal structure consists of the inorganic-framework of corner-sharing $[PbI_6]^{4-}$ octahedra with MA or GA as the A cation occupying the 12-fold coordinate cavities formed by eight $[PbI_6]^{4-}$

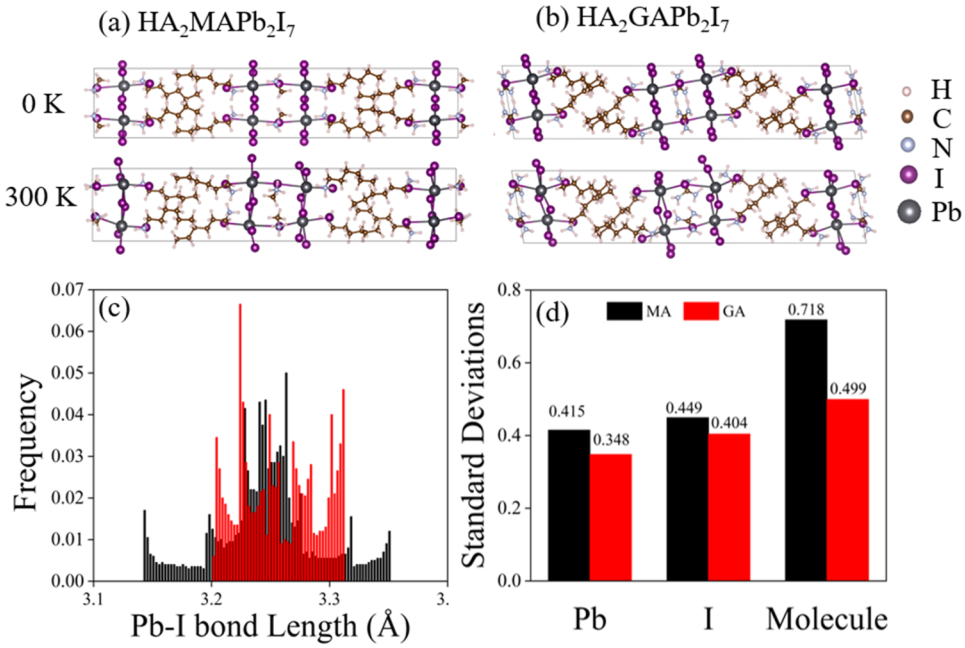

FIG. 1. Optimized geometries and a representative snapshot of the MD trajectory at 300 K of (a) $HA_2MAPb_2I_7$ and (b) $HA_2GAPb_2I_7$. (c) Histograms distributions of the Pb–I bond length and (d) standard deviations in the positions of Pb and I atoms and organic molecules computed over the 3 ps MD trajectories of the two perovskites at 300 K.

octahedra. HA are spacer cations separating the inorganic layers. The GA cation has an impact on the structure of the inorganic lattice due to its larger size. For instance, the calculated average values of the Pb–I–Pb angles in the optimized $HA_2MAPb_2I_7$ and $HA_2GAPb_2I_7$ structures are 153.14° and 159.04°, respectively. GA increases the Pb–I–Pb angle relative to MA, in agreement with the corresponding experimental values of 155.73° and 162.02°.[27] The average Pb–I bond lengths are 3.211 and 3.247 Å for the MA and GA perovskites, respectively. Compared with $HA_2MAPb_2I_7$, $HA_2GAPb_2I_7$ exhibits longer Pb–I bonds and larger Pb–I–Pb angles, demonstrating that the incorporation of large A cations distorts the inorganic lattice of the perovskites.

Figure 1(c) shows the distributions of the Pb–I bond lengths in the two systems at room temperature. The Pb–I bond length distribution is narrower in the GA perovskite, indicating that structural fluctuations are smaller and the movement of the Pb–I inorganic framework is inhibited by the larger GA cations, compared to the smaller MA cations. There is a lot of free space in the smaller-sized MA cation system, allowing for a wider range of inorganic frame movement. In comparison, in the GA perovskite system, the large GA cations inside the perovskite cage and the more compressed interlayer cations have a steric hindrance, which limits the movement of the inorganic framework.

In addition to the fluctuations of the bond length, we calculated standard deviations in the positions of the Pb and I atoms and the atoms of the organic molecules in the two perovskite systems, according to the equation $\sigma_i = \sqrt{\langle (\vec{r}_i - \langle \vec{r}_i \rangle)^2 \rangle}$, in which $\vec{r}_i$ represents the position of atom type i. The data, shown in Fig. 1(d), characterize the fluctuations of the atoms around their equilibrium positions. The standard deviations in the atomic positions are notably smaller in $HA_2GAPb_2I_7$ than $HA_2MAPb_2I_7$. The difference is particularly pronounced for the molecular GA vs MA species. The results show that MA cations have much more freedom to move around inside the inorganic cavities than GA cations and that the large-size A-site cation suppresses the atomic fluctuation of the inorganic lattice.

Because electrons and holes are supported by the inorganic lattice, the differences in the lattice structural dynamics between the smaller and larger cation perovskites have a direct influence on both electronic properties, such as the energy gap and wavefunction localization, and electron–vibrational interactions, including both inelastic and elastic electron–phonon scattering.

Figures 2(a) and 2(b) display the projected density of states (PDOS) of $HA_2MAPb_2I_7$ and $HA_2GAPb_2I_7$ separated into contributions of the Pb, I, HA, MA, and GA components. Similar to the 3D $MAPbI_3$ perovskite, the HOMO of the 2DRP perovskites is composed of I and Pb atomic orbitals, while the LUMO primarily consists of Pb atomic orbitals. The band edge states are all contributed by the inorganic groups. Hence, the organic cations in the 2DRP perovskites cannot directly affect the NA coupling and electron–hole recombination, but they can influence the bandgap, charge localization, and electron–vibrational interactions indirectly, by altering the $[PbI_6]^{4-}$ octahedral Pb–I framework. The HOMO and LUMO of $HA_2MAPb_2I_7$ are separated by a bandgap of 1.79 eV. When all A cations in the 2D perovskite are replaced with the larger-sized GA cations, the bandgap value is increased to 1.92 eV. The large-size GA cations cause the Pb–I–Pb bond angle to increase.

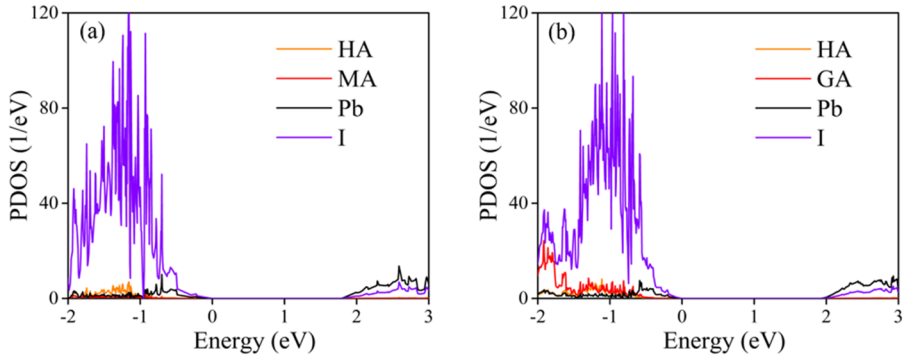

FIG. 2. Projected density of states (PDOS) of the optimized structure of (a) $HA_2MAPb_2I_7$ and (b) $HA_2GAPb_2I_7$, separated into contributions from Pb, I, HA, MA, and GA. Zero energy is set to the Fermi level.

Consequently, the overlap between the s orbital of Pb and the p orbital of I decreases, which results in the increase in the electronic bandgap. The calculated bandgaps show agreement with the onsets of experimental light absorption of 2.08 and 2.13 eV for the MA and GA 2DRP perovskites, respectively.

The factors that determine the nonradiative electron–hole recombination time in the NAMD simulation includes energy gap, NA coupling, and quantum coherence time. The bandgap values differ little between the two systems, as discussed above. The NA coupling plays a very important role. It reflects the sensitivity of the electronic wavefunctions to atomic displacements, $\langle \phi_{LUMO} | \nabla_R | \phi_{HOMO} \rangle$, and also, it depends on the localization of the initial and final wavefunctions. For the NA coupling to be large, the two wavefunctions should be localized in the same space and vary rapidly with atomic displacements. Figures 3(a) and 3(b) show the charge densities of HOMO and LUMO in the two systems in the optimized geometries. Even when the systems are cooled down to 0 K, a small symmetry breaking among layers causes partial localization of HOMO and LUMO and, therefore, separation of electron and hole, which reduces the NA coupling and extends carrier lifetimes.[77] In order to characterize the extent of localization of the electron and hole charge densities at the ambient temperature, we compute the inverse

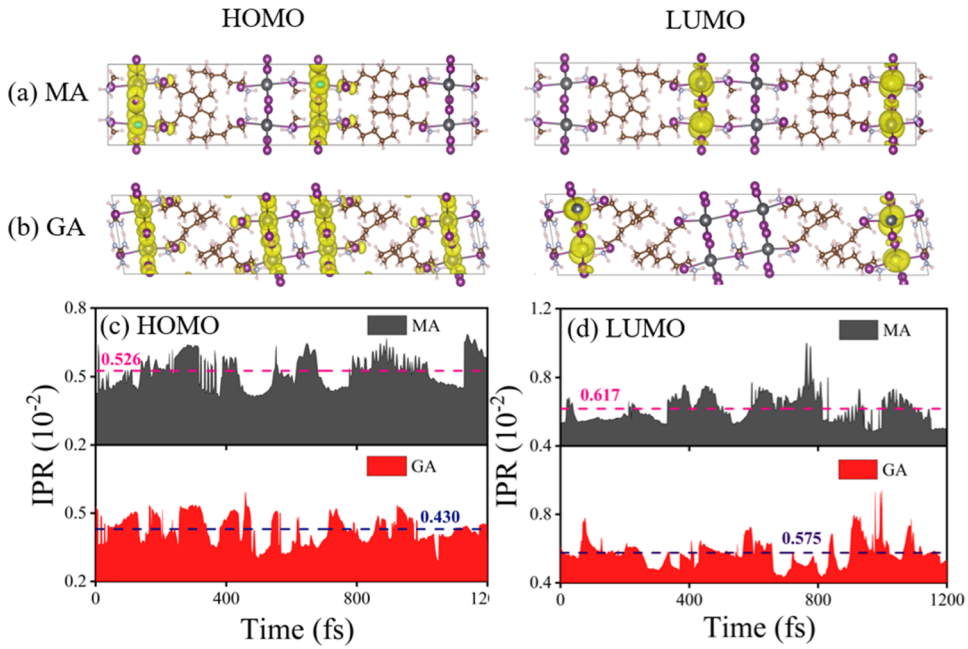

FIG. 3. HOMO and LUMO charge densities for optimized (a) $HA_2MAPb_2I_7$ and (b) $HA_2GAPb_2I_7$. Inverse participation ratio (IPR) of (c) HOMO and (d) LUMO of the two perovskites along the 2 ps trajectories at 300 K.

participation ratio (IPR) along a representative part of the MD trajectory in the two perovskite systems, Figs. 3(c) and 3(d). Given the expansion of the Kohn–Sham orbitals in the basis of N plane waves $|i\rangle$ with momentum $|k_i\rangle$, the IPR is defined as

$$\mathrm{IPR} = \mathrm{N} \cdot \frac{\sum \mathrm{k_i}^4}{\left(\sum \mathrm{k_i}^2\right)^2} \quad \mathrm{IPR} \in (0, 1].$$

Larger IPR values indicate more localized wavefunctions. As shown in Fig. 3(d), the canonically averaged IPR values for HOMO and LUMO are 5.26×10^{-3} and 6.17×10^{-3} in $HA_2MAPb_2I_7$, while these values are 4.20×10^{-3} and 5.75×10^{-3} in $HA_2MAPb_2I_7$, respectively. The IPR values are larger in the MA system, indicating that the charges are more localized. Electrons are more localized than holes in both systems. The more significant charge localization in $HA_2MAPb_2I_7$ compared to $HA_2GAPb_2I_7$ suggests reduced overlaps of electrons and holes and smaller NA coupling, as confirmed by the average absolute value reported in Table I, 0.33 vs 0.50 meV.

Compared to other systems,[57–59,63–69] the NA coupling values are small in lead-halide perovskites, because they are soft materials with heavy elements. Being soft, they undergo substantial thermal fluctuations, resulting in partial localization and reduced overlap of electron and hole wavefunctions.[78–80] The large masses of Pb and I atoms forming the inorganic lattice that supports the charges imply small atomic velocities, and the NA coupling is directly proportional to the atomic velocity.[81,82] The smaller value of the NA coupling in $HA_2MAPb_2I_7$ contributes to the longer charge carrier lifetime in this material, compared to $HA_2GAPb_2I_7$, Table I.

Both inelastic and elastic electron–vibrational scattering influences nonradiative electron–hole recombination. Characterized by the NA coupling, inelastic scattering results in the transfer of electronic energy to vibrations during the recombination process. Elastic electron–vibrational scattering causes loss of coherence within the electronic subsystem. In particular, quantum mechanical superpositions formed between HOMO and LUMO during the electronic transition are dampened due to elastic scattering. This process is known as decoherence in the time domain, and it is directly related to the Franck–Condon factor in the energy domain.[81] The limit of infinitely fast decoherence gives the quantum Zeno effect, as a result of which quantum transitions stop.[51,83–85]

TABLE I. Experimental bandgaps, average absolute nonadiabatic coupling, pure-dephasing time, energy gap fluctuation, and nonradiative electron–hole recombination time of $HA_2MAPb_2I_7$ and $HA_2GAPb_2I_7$.

	Bandgap (eV)	NA coupling (meV)	Dephasing (fs)	Bandgap fluctuation (eV^2)	Recombination (ps)
MA	2.08[27]	0.33	3.77	0.026	156
GA	2.13[27]	0.50	3.84	0.025	57

The decoherence time is calculated as the pure-dephasing time of optical response theory in the second order cumulant approximation,[49,50]

$$\mathrm{D_{ij}}(t) = \exp\left(-\frac{1}{\hbar}\int_0^{\mathrm{t}} \mathrm{dt}' \int_0^{t'} dt'' C_{ij}(t'') \right).$$

Here, $C_{ij}(t)$ is the unnormalized autocorrelation function (ACF) of thermal fluctuations of the HOMO–LUMO energy gap, $\delta E_{ij}(t)$,

$$\mathrm{C_{ij}(t)} = \left\langle \delta \mathrm{E_{ij}}(\mathrm{t}') \delta E_{ij}(t - t') \right\rangle_{t'}.$$

The ACF initial value, $C_{ij}(0)$, gives the energy gap fluctuation, and a large fluctuation leads to rapid decoherence. The pure-dephasing times and the bandgap fluctuations are presented in Table I. The pure-dephasing times are obtained by Gaussian fitting the pure-dephasing functions, $\exp\left[-0.5(t/\tau)^2\right]$. There is a small difference between the pure-dephasing times of $HA_2MAPb_2I_7$ and $HA_2GAPb_2I_7$. The coherence times are short, suggesting that the system approaches the quantum Zeno regime,[51,83–85] which favors long charge carrier lifetimes. The pure-dephasing functions and the ACFs are shown in Fig. 4(b).

Fourier transforms of the ACFs of the phonon-induced fluctuations of the electronic bandgap provide the spectral density, also known as the influence spectrum,[86] which characterizes the vibrational modes that couple to the electronic transitions. The signal intensity at a given frequency is proportional to the strength of the coupling of the electronic subsystem to the vibration with that frequency. Figure 4(a) shows that the influence spectra, corresponding to the nonradiative electron–hole recombination in the 2DRP perovskite systems, are dominated by low-frequency vibrations. The peak at 20 cm^{-1} may be associated with the $[PbI_6]^{4-}$ octahedral distortion,[87] and the peak at 100 cm^{-1} can be assigned to the stretching of Pb–I bonds.[88] The higher frequency modes in the 200–400 cm^{-1} range are attributed to the torsional modes of the organic cations.[88] The interaction of MA cations with the inorganic framework may cause the torsional mode of the MA cations to shift to a higher frequency, forming the peak at 420 cm^{-1}, Fig. 4(a).[88] The larger GA cation is too constrained inside the inorganic Pb–I lattice to exhibit this motion, and for this reason, the corresponding peak is not observed in the $HA_2GAPb_2I_7$ influence spectrum. It is interesting to note that motions of the A-site cations contribute to the nonradiative electron–hole recombination even though they make no contributions to the electron and hole wavefunctions near the bandgap, Fig. 2. The A-site cations can couple to the charge carriers through electrostatic interactions, and indirectly by altering the structure of the inorganic lattice.

Figure 5 demonstrates the nonradiative electron–hole recombination dynamics. It shows the decay of the population of the excited electronic state in $HA_2MAPb_2I_7$ and $HA_2GAPb_2I_7$ obtained by the NAMD simulation. The nonradiative charge recombination is faster in the MA system compared to the GA perovskite, in agreement with the experiments.[27] Following a short Gaussian like decay regime, present in all quantum systems and associated with the quantum Zeno effect,[51,83–85] the decay is approximately exponential. Fitting the data to the short-time linear approximation of the exponential decay, $\mathrm{P(t)} = \exp(-\mathrm{t}/\tau) \approx 1 - \mathrm{t}/\tau$, gives the recombination times

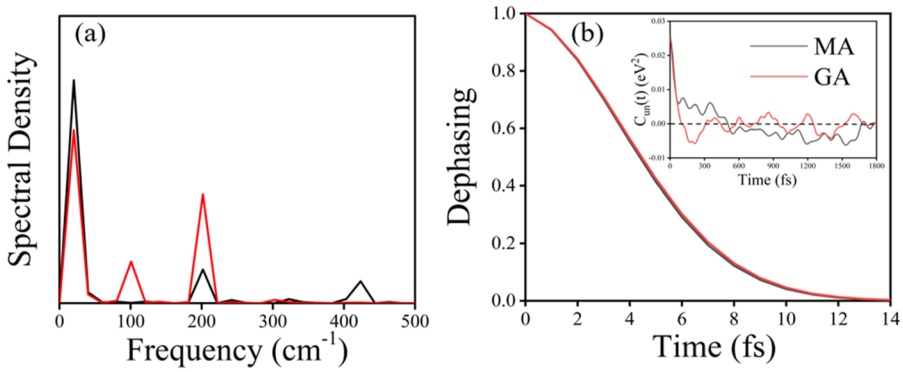

FIG. 4. (a) Spectral densities obtained by Fourier transforms of autocorrelation functions of fluctuations of bandgap in $HA_2MAPb_2I_7$ and $HA_2GAPb_2I_7$. (b) Pure-dephasing functions for the HOMO–LUMO transition in the two perovskites. The inset shows the unnormalized autocorrelation functions.

reported in Table I. The lifetime ratio is slightly less than 3, in agreement with the experimentally reported factor of two lifetime shortening upon incorporation of large GA cations.[27]

The difference in the nonradiative electron–hole recombination times in the $HA_2MAPb_2I_7$ and $HA_2GAPb_2I_7$ perovskites arises from the NA coupling values, Table I. According to perturbation theory, such as Fermi's golden rule, the transition rate is proportional to the coupling squared, explaining the change in the lifetime. The other two factors, energy gap and decoherence time, vary little between the two systems. The dependence of transition time on coherence time can be strong,[51] and the slightly shorter coherence time for $HA_2MAPb_2I_7$ also contributes to the longer lifetime. Since the NA coupling is the main factor rationalizing the dependence of the electron–hole recombination time on the A-site cation, it is important to know the origin of the difference in the NA coupling values. The NA coupling is larger in $HA_2GAPb_2I_7$ than $HA_2MAPb_2I_7$ because thermal fluctuations are suppressed in the former system, Figs. 1(c) and 1(d). The large GA cations create a significant hindrance to atomic motions, while MA cations can move much more freely inside the cages formed by the inorganic Pb–I lattice. Thermal atomic disorder leads to partial localization of electrons and holes, Figs. 3(c) and 3(d), reduces their overlap, decreases the NA coupling, and enhances the carrier lifetime.

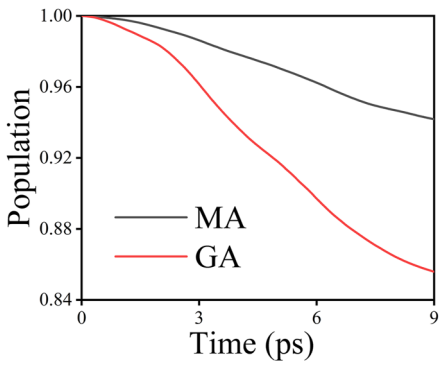

FIG. 5. Electron–hole recombination dynamics in $HA_2MAPb_2I_7$ and $HA_2GAPb_2I_7$.

One observes opposite trends between the 3D perovskites in which only a fraction of MA cations can be replaced with GA cations,[31–33] and the 2DRP perovskites that allow full replacement of MA with GA.[27,34–36] The difference can be rationalized by structural disorder and partial charge localization as well. Replacement of some MA with GA creates disorder, increases charge localization, and extends charge lifetime. Complete replacement of MA with GA reduces disorder by suppressing thermal structural fluctuations, makes charges more delocalized, and shortens their lifetime. These facts highlight once again the strong influence of structural disorder on charge carriers in metal halide perovskites.

IV. CONCLUSION

In conclusion, we have studied the nonradiative electron–hole recombination dynamics in pristine $HA_2MAPb_2I_7$ and $HA_2GAPb_2I_7$ perovskites by combining *ab initio* TDDFT and NAMD. The calculated nonradiative recombination occurs faster in the GA system relative to the MA perovskite, in agreement with experiment. The large GA cations create a steric hindrance that suppresses thermal structural fluctuations. As a result, electron and hole wavefunctions remain more delocalized at a finite temperature, and the NA coupling is larger in the GA perovskite, accelerating nonradiative charge recombination. For the same reason, the transition dipole moment between HOMO and LUMO should increase when MA cations are replaced by GA, and radiative charge recombination should be faster as well. The situation is opposite to that observed upon doping large-sized A-site cations into 3D perovskites. This is because 3D perovskite structures cannot accommodate large structural distortions, compared to 2D perovskites, and only a fraction of MA cations can be replaced by the larger GA cations in 3D without altering the crystal structure. Mixing of MA and GA cations in 3D enhances disorder, makes electrons and holes more localized, and reduces their interaction and recombination. A similar effect should be observed in 2D, if only a fraction of MA cations is replaced by GA. Extending carrier lifetimes is usually desirable, since typically it leads to a better material performance. The reported study provides important fundamental insights into the unusual structure–property relationships of metal halide

perovskites, guiding design, and synthesis of advanced structures and materials.

SUPPLEMENTARY MATERIAL

The supplementary material contains the coordinates of the optimized structures of the two systems under investigation.

ACKNOWLEDGMENTS

This work was supported by the National Natural Science Foundation of China (Grant No. 92372121). O.V.P. acknowledges the support of the US National Science Foundation (Grant No. CHE-2154367).

AUTHOR DECLARATIONS

Conflict of Interest

The authors have no conflicts to disclose.

Author Contributions

Dandan Dai: Data curation (equal); Investigation (equal); Software (equal); Writing – original draft (equal). **Sraddha Agrawal**: Investigation (equal); Methodology (equal); Writing – review & editing (equal). **Oleg V. Prezhdo**: Conceptualization (equal); Funding acquisition (equal); Methodology (equal); Project administration (equal); Supervision (equal); Writing – review & editing (equal). **Run Long**: Conceptualization (equal); Funding acquisition (equal); Methodology (equal); Project administration (equal); Supervision (equal); Writing – review & editing (equal).

DATA AVAILABILITY

The data that support the findings of this study are available from the corresponding authors upon reasonable request.

REFERENCES

[1]M. Gratzel, "The rise of highly efficient and stable perovskite solar cells," Acc. Chem. Res. **50**, 487–491 (2017).
[2]J. P. Correa-Baena, M. Saliba, T. Buonassisi, M. Gratzel, A. Abate, W. Tress, and A. Hagfeldt, "Promises and challenges of perovskite solar cells," Science **358**, 739–744 (2017).
[3]A. Kojima, K. Teshima, Y. Shirai, and T. Miyasaka, "Organometal halide perovskites as visible-light sensitizers for photovoltaic cells," J. Am. Chem. Soc. **131**, 6050 (2009).
[4]National Renewable Energy Laboratory (NREL), Best research cell efficiency chart, https://Www.Nrel.Gov/Pv/Cell-Efficiency.Html (accessed 06 November 2020).
[5]Y. S. Guo, O. Yaffe, T. D. Hull, J. S. Owen, D. R. Reichman, and L. E. Brus, "Dynamic emission Stokes shift and liquid-like dielectric solvation of band edge carriers in lead-halide perovskites," Nat. Commun. **10**, 1175 (2019).
[6]H. J. Snaith, "Perovskites: The emergence of a new era for low-cost, high-efficiency solar cells," J. Phys. Chem. Lett. **4**, 3623–3630 (2013).
[7]H. Kim, K.-G. Lim, and T.-W. Lee, "Planar heterojunction organometal halide perovskite solar cells: Roles of interfacial layers," Energy Environ. Sci. **9**, 12–30 (2016).
[8]A. L. Efros and L. E. Brus, "Nanocrystal quantum dots: From discovery to modern development," ACS Nano **15**, 6192–6210 (2021).
[9]W. J. Yin, T. T. Shi, and Y. F. Yan, "Unusual defect physics in $CH_3NH_3PbI_3$ perovskite solar cell absorber," Appl. Phys. Lett. **104**, 063903 (2014).
[10]W. J. Yin, T. Shi, and Y. Yan, "Unique properties of halide perovskites as possible origins of the superior solar cell performance," Adv. Mater. **26**, 4653–4658 (2014).
[11]G. C. Xing, N. Mathews, S. Y. Sun, S. S. Lim, Y. M. Lam, M. Gratzel, S. Mhaisalkar, and T. C. Sum, "Long-range balanced electron- and hole-transport lengths in organic–inorganic $CH_3NH_3PbI_3$," Science **342**, 344–347 (2013).
[12]D. W. deQuilettes, S. M. Vorpahl, S. D. Stranks, H. Nagaoka, G. E. Eperon, M. E. Ziffer, H. J. Snaith, and D. S. Ginger, "Impact of microstructure on local carrier lifetime in perovskite solar cells," Science **348**, 683–686 (2015).
[13]D. Shi, V. Adinolfi, R. Comin, M. J. Yuan, E. Alarousu, A. Buin, Y. Chen, S. Hoogland, A. Rothenberger, K. Katsiev, Y. Losovyj, X. Zhang, P. A. Dowben, O. F. Mohammed, E. H. Sargent, and O. M. Bakr, "Low trap-state density and long carrier diffusion in organolead trihalide perovskite single crystals," Science **347**, 519–522 (2015).
[14]D. Yang, X. Zhou, R. Yang, Z. Yang, W. Yu, X. Wang, C. Li, S. Liu, and R. P. H. Chang, "Surface optimization to eliminate hysteresis for record efficiency planar perovskite solar cells," Energy Environ. Sci. **9**, 3071–3078 (2016).
[15]V. D'Innocenzo, G. Grancini, M. J. Alcocer, A. R. Kandada, S. D. Stranks, M. M. Lee, G. Lanzani, H. J. Snaith, and A. Petrozza, "Excitons versus free charges in organo-lead tri-halide perovskites," Nat. Commun. **5**, 3586 (2014).
[16]B. Saparov and D. B. Mitzi, "Organic–inorganic perovskites: Structural versatility for functional materials design," Chem. Rev. **116**, 4558–4596 (2016).
[17]K. Galkowski, A. Mitioglu, A. Miyata, P. Plochocka, O. Portugall, G. E. Eperon, J. T.-W. Wang, T. Stergiopoulos, S. D. Stranks, H. J. Snaith, and R. J. Nicholas, "Determination of the exciton binding energy and effective masses for methylammonium and formamidinium lead tri-halide perovskite semiconductors," Energy Environ. Sci. **9**, 962–970 (2016).
[18]C. C. Stoumpos, C. D. Malliakas, and M. G. Kanatzidis, "Semiconducting tin and lead iodide perovskites with organic cations: Phase transitions, high mobilities, and near-infrared photoluminescent properties," Inorg. Chem. **52**, 9019–9038 (2013).
[19]M. D. Smith and H. I. Karunadasa, "White-light emission from layered halide perovskites," Acc. Chem. Res. **51**, 619–627 (2018).
[20]Y. S. Guo, O. Yaffe, D. W. Paley, A. N. Beecher, T. D. Hull, G. Szpak, J. S. Owen, L. E. Brus, and M. A. Pimenta, "Interplay between organic cations and inorganic framework and incommensurability in hybrid lead-halide perovskite $CH_3NH_3PbBr_3$," Phys. Rev. Mater. **1**, 042401 (2017).
[21]W. Travis, E. N. K. Glover, H. Bronstein, D. O. Scanlon, and R. G. Palgrave, "On the application of the tolerance factor to inorganic and hybrid halide perovskites: A revised system," Chem. Sci. **7**, 4548–4556 (2016).
[22]G. Kieslich, S. Sun, and A. K. Cheetham, "Solid-state principles applied to organic–inorganic perovskites: New tricks for an old dog," Chem. Sci. **5**, 4712–4715 (2014).
[23]C. C. Stoumpos, L. Mao, C. D. Malliakas, and M. G. Kanatzidis, "Structure–band gap relationships in hexagonal polytypes and low-dimensional structures of hybrid tin iodide perovskites," Inorg. Chem. **56**, 56–73 (2016).
[24]C. Katan, N. Mercier, and J. Even, "Quantum and dielectric confinement effects in lower-dimensional hybrid perovskite semiconductors," Chem. Rev. **119**, 3140–3192 (2019).
[25]L. Mao, C. C. Stoumpos, and M. G. Kanatzidis, "Two-dimensional hybrid halide perovskites: Principles and promises," J. Am. Chem. Soc. **141**, 1171–1190 (2019).
[26]M. Kepenekian, B. Traore, J. C. Blancon, L. Pedesseau, H. Tsai, W. Nie, C. C. Stoumpos, M. G. Kanatzidis, J. Even, A. D. Mohite, S. Tretiak, and C. Katan, "Concept of lattice mismatch and emergence of surface states in two-dimensional hybrid perovskite quantum wells," Nano Lett. **18**, 5603–5609 (2018).
[27]Y. Fu, M. P. Hautzinger, Z. Luo, F. Wang, D. Pan, M. M. Aristov, I. A. Guzei, A. Pan, X. Zhu, and S. Jin, "Incorporating large a cations into lead iodide perovskite cages: Relaxed Goldschmidt tolerance factor and impact on exciton–phonon interaction," ACS Cent. Sci. **5**, 1377–1386 (2019).
[28]O. Yaffe, Y. S. Guo, L. Z. Tan, D. A. Egger, T. Hull, C. C. Stoumpos, F. Zheng, T. F. Heinz, L. Kronik, M. G. Kanatzidis, J. S. Owen, A. M. Rappe, M. A. Pimenta,

and L. E. Brus, "Local polar fluctuations in lead halide perovskite crystals," Phys. Rev. Lett. **118**, 136001 (2017).
[29]L. M. Herz, "How lattice dynamics moderate the electronic properties of metal-halide perovskites," J. Phys. Chem. Lett. **9**, 6853–6863 (2018).
[30]D. A. Egger, A. Bera, D. Cahen, G. Hodes, T. Kirchartz, L. Kronik, R. Lovrincic, A. M. Rappe, D. R. Reichman, and O. Yaffe, "What remains unexplained about the properties of halide perovskites?," Adv. Mater. **30**, e1800691 (2018).
[31]J. He, W.-H. Fang, R. Long, and O. V. Prezhdo, "Increased lattice stiffness suppresses nonradiative charge recombination in $MAPbI_3$ doped with larger cations: Time-domain ab initio analysis," ACS Energy Lett. **3**, 2070–2076 (2018).
[32]N. De Marco, H. P. Zhou, Q. Chen, P. Y. Sun, Z. H. Liu, L. Meng, E. P. Yao, Y. S. Liu, A. Schiffer, and Y. Yang, "Guanidinium: A route to enhanced carrier lifetime and open-circuit voltage in hybrid perovskite solar cells," Nano Lett. **16**, 1009–1016 (2016).
[33]S. P. Pang, H. Hu, J. L. Zhang, S. L. Lv, Y. M. Yu, F. Wei, T. S. Qin, H. X. Xu, Z. H. Liu, and G. L. Cui, "$NH_2CH{=}NH_2PbI_3$: An alternative organolead iodide perovskite sensitizer for mesoscopic solar cells," Chem. Mater. **26**, 1485–1491 (2014).
[34]M. P. Hautzinger, D. Pan, A. K. Pigg, Y. Fu, D. J. Morrow, M. Leng, M.-Y. Kuo, N. Spitha, D. P. Lafayette, D. D. Kohler, J. C. Wright, and S. Jin, "Band edge tuning of two-dimensional Ruddlesden–Popper perovskites by a cation size revealed through nanoplates," ACS Energy Lett. **5**, 1430–1437 (2020).
[35]X. Li, Y. Fu, L. Pedesseau, P. Guo, S. Cuthriell, I. Hadar, J. Even, C. Katan, C. C. Stoumpos, R. D. Schaller, E. Harel, and M. G. Kanatzidis, "Negative pressure engineering with large cage cations in 2D halide perovskites causes lattice softening," J. Am. Chem. Soc. **142**, 11486–11496 (2020).
[36]Y. Fu, X. Jiang, X. Li, B. Traore, I. Spanopoulos, C. Katan, J. Even, M. G. Kanatzidis, and E. Harel, "Cation engineering in two-dimensional Ruddlesden–Popper lead iodide perovskites with mixed large A-site cations in the cages," J. Am. Chem. Soc. **142**, 4008–4021 (2020).
[37]E. Runge and E. K. U. Gross, "Density-functional theory for time-dependent systems," Phys. Rev. Lett. **52**, 997–1000 (1984).
[38]W. Kohn and L. J. Sham, "Self-consistent equations including exchange and correlation effects," Phys. Rev. **140**, A1133–A1138 (1965).
[39]C. F. Craig, W. R. Duncan, and O. V. Prezhdo, "Trajectory surface hopping in the time-dependent Kohn–Sham approach for electron–nuclear dynamics," Phys. Rev. Lett. **95**, 163001 (2005).
[40]R. Crespo-Otero and M. Barbatti, "Recent advances and perspectives on nonadiabatic mixed quantum–classical dynamics," Chem. Rev. **118**, 7026–7068 (2018).
[41]B. F. E. Curchod and T. J. Martínez, "Ab initio nonadiabatic quantum molecular dynamics," Chem. Rev. **118**, 3305–3336 (2018).
[42]S. Mai, P. Marquetand, and L. González, "Nonadiabatic dynamics: The SHARC approach," Wiley Interdiscip. Rev.: Comput. Mol. Sci. **8**, e1370 (2018).
[43]Q. J. Zheng, W. B. Chu, C. Y. Zhao, L. L. Zhang, H. L. Guo, Y. N. Wang, X. Jiang, and J. Zhao, "Ab initio nonadiabatic molecular dynamics investigations on the excited carriers in condensed matter systems," Wiley Interdiscip. Rev.: Comput. Mol. Sci. **9**, e1411 (2019).
[44]L. J. Wang, A. Akimov, and O. V. Prezhdo, "Recent progress in surface hopping: 2011–2015," J. Phys. Chem. Lett. **7**, 2100–2112 (2016).
[45]O. V. Prezhdo, "Modeling non-adiabatic dynamics in nanoscale and condensed matter systems," Acc. Chem. Res. **54**, 4239–4249 (2021).
[46]J. C. Tully, "Molecular dynamics with electronic transitions," J. Chem. Phys. **93**, 1061–1071 (1990).
[47]E. R. Bittner and P. J. Rossky, "Quantum decoherence in mixed quantum–classical systems: Nonadiabatic processes," J. Chem. Phys. **103**, 8130–8143 (1995).
[48]B. F. Habenicht and O. V. Prezhdo, "Nonradiative quenching of fluorescence in a semiconducting carbon nanotube: A time-domain *ab initio* study," Phys. Rev. Lett. **100**, 197402 (2008).
[49]S. Mukamel, Principles of Nonlinear Optical Spectroscopy (Oxford University Press, 1995).
[50]A. V. Akimov and O. V. Prezhdo, "Persistent electronic coherence despite rapid loss of electron–nuclear correlation," J. Phys. Chem. Lett. **4**, 3857–3864 (2013).
[51]S. Gumber and O. V. Prezhdo, "Zeno and anti-Zeno effects in nonadiabatic molecular dynamics," J. Phys. Chem. Lett. **14**, 7274–7282 (2023).
[52]L. Qiao, W. H. Fang, R. Long, and O. V. Prezhdo, "Photoinduced dynamics of charge carriers in metal halide perovskites from an atomistic perspective," J. Phys. Chem. Lett. **11**, 7066–7082 (2020).
[53]L. Liu, W.-H. Fang, R. Long, and O. V. Prezhdo, "Lewis base passivation of hybrid halide perovskites slows electron–hole recombination: Time-domain ab initio analysis," J. Phys. Chem. Lett. **9**, 1164–1171 (2018).
[54]D. Strandell, Y. F. Wu, C. Mora-Perez, O. Prezhdo, and P. Kambhampati, "Breaking the Condon approximation for light emission from metal halide perovskite nanocrystals," J. Phys. Chem. Lett. **14**, 11281–11285 (2023).
[55]D. Y. Liu, Y. F. Wu, A. S. Vasenko, and O. V. Prezhdo, "Grain boundary sliding and distortion on a nanosecond timescale induce trap states in $CsPbBr_3$: *Ab initio* investigation with machine learning force field," Nanoscale **15**, 285–293 (2023).
[56]R. Shi, Z. Zhang, W.-H. Fang, and R. Long, "Charge localization control of electron–hole recombination in multilayer two-dimensional Dion–Jacobson hybrid perovskites," J. Mater. Chem. A **8**, 9168–9176 (2020).
[57]Y. H. Zhu, O. V. Prezhdo, R. Long, and W. H. Fang, "Twist angle-dependent intervalley charge carrier transfer and recombination in bilayer WS_2," J. Am. Chem. Soc. **145**, 22826–22835 (2023).
[58]L. Q. Li, R. Long, and O. V. Prezhdo, "Why chemical vapor deposition grown MoS_2 samples outperform physical vapor deposition samples: Time-domain ab initio analysis," Nano Lett. **18**, 4008–4014 (2018).
[59]C. Xu, N. Barden, E. M. Alexeev, X. L. Wang, R. Long, A. R. Cadore, I. Paradisanos, A. K. Ott, G. Soavi, S. Tongay, G. Cerullo, A. C. Ferrari, O. V. Prezhdo, and Z. H. Loh, "Ultrafast charge transfer and recombination dynamics in monolayer-multilayer WSe_2 Junctions revealed by time-resolved photoemission electron microscopy," ACS Nano **18**, 1931–1947 (2024).
[60]Z. Zhang, J. He, and R. Long, "Ultrafast charge separation and recombination across a molecule/$CsPbBr_3$ quantum dot interface from first-principles nonadiabatic molecular dynamics simulation," J. Phys. Chem. C **123**, 23800–23806 (2019).
[61]H. Baker, C. M. Perez, C. Sonnichsen, D. Strandell, O. V. Prezhdo, and P. Kambhampati, "Breaking phonon bottlenecks through efficient Auger processes in perovskite nanocrystals," ACS Nano **17**, 3913–3920 (2023).
[62]D. Strandell, C. Mora Perez, Y. F. Wu, O. V. Prezhdo, and P. Kambhampati, "Excitonic quantum coherence in light emission from $CsPbBr_3$ metal-halide perovskite nanocrystals," Nano Lett. **24**, 61–66 (2023).
[63]L. L. Zhang, A. S. Vasenko, J. Zhao, and O. V. Prezhdo, "Mono-elemental properties of 2D black phosphorus ensure extended charge carrier lifetimes under oxidation: Time-domain ab initio analysis," J. Phys. Chem. Lett. **10**, 1083 (2019).
[64]S. Agrawal, A. S. Vasenko, D. J. Trivedi, and O. V. Prezhdo, "Charge carrier nonadiabatic dynamics in non-metal doped graphitic carbon nitride," J. Chem. Phys. **156**, 000156 (2022).
[65]W. Stier, W. R. Duncan, and O. V. Prezhdo, "Thermally assisted sub-10 fs electron transfer in dye-sensitized nanocrystalline TiO_2 solar cells," Adv. Mater. **16**, 240 (2004).
[66]Z. S. Zhang, L. H. Liu, W. H. Fang, R. Long, M. V. Tokina, and O. V. Prezhdo, "Plasmon-mediated electron injection from Au nanorods into MoS_2: Traditional versus photoexcitation mechanism," Chem **4**, 1112–1127 (2018).
[67]S. Mondal, U. Chowdhury, S. Dey, M. Habib, C. Mora Perez, T. Frauenheim, R. Sarkar, S. Pal, and O. V. Prezhdo, "Controlling charge carrier dynamics in porphyrin nanorings by optically active templates," J. Phys. Chem. Lett. **14**, 11384–11392 (2023).
[68]Y. W. Fu, K. J. Lu, A. L. Hu, J. Huang, L. J. Guo, J. Zhou, J. Zhao, O. V. Prezhdo, and M. C. Liu, "d_{Z^2} band links frontier orbitals and charge carrier dynamics of single-atom cocatalyst-aided photocatalytic H_2 production," J. Am. Chem. Soc. **145**, 28166–28175 (2023).
[69]Z. B. Zhou, Z. F. Zheng, J. J. He, J. L. Wang, O. V. Prezhdo, and T. Frauenheim, "Ultrafast laser control of antiferromagnetic-ferrimagnetic switching in two-dimensional ferromagnetic semiconductor heterostructures," Nano Lett. **23**, 5688–5695 (2023).
[70]G. Kresse and J. Furthmuller, "Efficient iterative schemes for *ab initio* total-energy calculations using a plane-wave basis set," Phys. Rev. B **54**, 11169–11186 (1996).
[71]J. P. Perdew, K. Burke, and M. Ernzerhof, "Generalized gradient approximation made simple," Phys. Rev. Lett. **77**, 3865–3868 (1996).

[72]P. E. Blochl, "Projector augmented-wave method," Phys. Rev. B **50**, 17953–17979 (1994).
[73]H. J. Monkhorst and J. D. Pack, "Special points for Brillouin-zone integrations," Phys. Rev. B **13**, 5188–5192 (1976).
[74]S. Grimme, S. Ehrlich, and L. Goerigk, "Effect of the damping function in dispersion corrected density functional theory," J. Comput. Chem. **32**, 1456–1465 (2011).
[75]W. B. Chu, Q. J. Zheng, A. V. Akimov, J. Zhao, W. A. Saidi, and O. V. Prezhdo, "Accurate computation of nonadiabatic coupling with projector augmented-wave pseudopotentials," J. Phys. Chem. Lett. **11**, 10073–10080 (2020).
[76]W. B. Chu and O. V. Prezhdo, "Concentric approximation for fast and accurate numerical evaluation of nonadiabatic coupling with projector augmented-wave pseudopotentials," J. Phys. Chem. Lett. **12**, 3082–3089 (2021).
[77]R. Shi, R. Long, W. H. Fang, and O. V. Prezhdo, "Rapid interlayer charge separation and extended carrier lifetimes due to spontaneous symmetry breaking in organic and mixed organic–inorganic Dion–Jacobson perovskites," J. Am. Chem. Soc. **145**, 5297–5309 (2023).
[78]W. B. Chu, W. A. Saidi, J. Zhao, and O. V. Prezhdo, "Soft lattice and defect covalency rationalize tolerance of β-$CsPbI_3$ perovskite solar cells to native defects," Angew. Chem., Int. Ed. **59**, 6435–6441 (2020).
[79]W. Li, A. S. Vasenko, J. F. Tang, and O. V. Prezhdo, "Anharmonicity extends carrier lifetimes in lead halide perovskites at elevated temperatures," J. Phys. Chem. Lett. **10**, 6219–6226 (2019).
[80]R. Shi, Q. Fang, A. S. Vasenko, R. Long, W. H. Fang, and O. V. Prezhdo, "Structural disorder in higher-temperature phases increases charge carrier lifetimes in metal halide perovskites," J. Am. Chem. Soc. **144**, 19137–19149 (2022).
[81]O. V. Prezhdo and P. J. Rossky, "Evaluation of quantum transition rates from quantum–classical molecular dynamics simulations," J. Chem. Phys. **107**, 5863–5878 (1997).
[82]A. V. Akimov and O. V. Prezhdo, "The pyxaid program for non-adiabatic molecular dynamics in condensed matter systems," J. Chem. Theory Comput. **9**, 4959–4972 (2013).
[83]B. Misra and E. C. G. Sudarshan, "The Zeno's paradox in quantum theory," J. Math. Phys. **18**, 756–763 (1977).
[84]O. V. Prezhdo, "Quantum anti-Zeno acceleration of a chemical reaction," Phys. Rev. Lett. **85**, 4413–4417 (2000).
[85]S. V. Kilina, A. J. Neukirch, B. F. Habenicht, D. S. Kilin, and O. V. Prezhdo, "Quantum Zeno effect rationalizes the phonon bottleneck in semiconductor quantum dots," Phys. Rev. Lett. **110**, 180404 (2013).
[86]G. Goodyear and R. M. Stratt, "The short-time intramolecular dynamics of solutes in liquids. II. Vibrational population relaxation," J. Chem. Phys. **107**, 3098–3120 (1997).
[87]A. M. A. Leguy, A. R. Goni, J. M. Frost, J. Skelton, F. Brivio, X. Rodriguez-Martinez, O. J. Weber, A. Pallipurath, M. I. Alonso, M. Campoy-Quiles, M. T. Weller, J. Nelson, A. Walsh, and P. R. F. Barnes, "Dynamic disorder, phonon lifetimes, and the assignment of modes to the vibrational spectra of methylammonium lead halide perovskites," Phys. Chem. Chem. Phys. **18**, 27051–27066 (2016).
[88]C. Quarti, G. Grancini, E. Mosconi, P. Bruno, J. M. Ball, M. M. Lee, H. J. Snaith, A. Petrozza, and F. De Angelis, "The Raman spectrum of the $CH_3NH_3PbI_3$ hybrid perovskite: Interplay of theory and experiment," J. Phys. Chem. Lett. **5**, 279–284 (2014).